

Hepatic Steatosis and Fibrosis in Obese, Dysmetabolic and Diabetic Nonhuman Primates Quantified by Noninvasive Echography

Yongqiang Liu¹, Haihua Gu², Hui Wang¹, Bingdi Wang¹, Xiaoli Wang¹, George Aoyagi², Yong-Fu Xiao¹, Keefe Chng², Xing Gao³, Jinhu Wang⁴, Eiketsu Sho⁵, Yao-Ping Lin⁶ and Yi Xin (Jim) Wang^{1,2*}

¹Crown Bioscience, Inc. Taicang, China

²Crown Bioscience, Inc. Louisiana, USA

³Department of Internal Medicine, Taicang Affiliated Hospital of Nanjing University of Traditional Chinese Medicine, China

⁴Department of Laboratory Medicine, Taicang Affiliated Hospital of Soochow University, China

⁵KCI Biotech, China

⁶School of Medicine, National Yang-Ming University, Taiwan

*Corresponding author: Yi-Xin (Jim) Wang, Cardiovascular and Metabolic Diseases Division, Crown Bioscience Inc., 6 West Beijing Road, Science & Technology Park Taicang Economic Development Area Jiangsu Province, China, Tel: +86-13915790818; Fax: +86-52153879801; E-mail: yxwang@crownbio.com

Received date: October 03, 2017; Accepted date: October 07, 2017; Published date: October 13, 2017

Copyright: © 2017 Liu Y, et al. This is an open-access article distributed under the terms of the Creative Commons Attribution License, which permits unrestricted use, distribution, and reproduction in any medium, provided the original author and source are credited.

Abstract

Purpose: Patients with obesity and type 2 diabetes (T2D) are more susceptible to the occurrence of nonalcoholic fatty liver disease (NAFLD)/steatohepatitis (NASH). Although liver biopsy is still reviewed as a gold standard for the diagnosis, due to its invasiveness, high cost and variable readouts, it has limited application in large scale clinical investigation and long term following up the therapeutic benefits. This study was to apply a clinically used noninvasive echography to quantitatively evaluate the NAFLD/NASH model in dysmetabolic nonhuman primates.

Method: Noninvasive echography with computer-assisted imaging analysis was used to quantify hepatic pathological changes in 36 cynomolgus monkeys at different dysmetabolic stage.

Result: Both hepatic/renal echo-intensity ratio (H/R=1.69 ± 0.12 vs 1.36 ± 0.09) and hepatic echo-intensity attenuation rate (HA=25.7 ± 5.7 vs 12.0 ± 3.2 kHz/cm) were significantly higher in obese (n=14) compared to control (n=22) monkeys, which were highly correlated with multiple metabolic risks such as obese, hyperlipidemia and liver fibrosis indices including body mass index (BMI), Alanine/Aspartate Transaminase (AST/ALT) and diabetes (BARD) score, fibrosis-4 (FIB4), AST to platelet ratio index (APRI), etc. Postmortem examination of liver biopsy tissue revealed liver pathology resembling human NAFLD/NASH and higher triglycerides (245 ± 26 vs 101 ± 32 mg/100 g tissue) in diabetic than control monkeys.

Conclusion: The data demonstrate for the first time that obese, dysmetabolic and diabetic monkeys can develop NAFLD/NASH assembling to human disease. The noninvasive and quantitative echography along with the nonhuman primate model can be used as a powerful translational tool for following-up disease progression, and evaluation of novel therapies for NAFLD/NASH both clinically and pre-clinically.

Keywords: NAFLD/NASH; Obese; Diabetes; Ultrasound; Nonhuman primates

Introduction

Nonalcoholic fatty liver disease (NAFLD)/steatohepatitis (NASH) is one of the most common causes of chronic liver disease and is a major public health problem worldwide [1-3]. The prevalence of NAFLD/NASH in the general population is approximately 20-30/5-12% [4]; however, in patients with obesity and type 2 diabetes (T2D), NAFLD is substantially more common, affecting up to 70% of patients [5,6]. Although the pathogenesis of NAFLD/NASH remains to be fully elucidated, one of the theories is “multiple parallel hits” including insulin resistance resulting in increased free fatty acid synthesis and uptake in the early stages of NAFLD, followed by oxidative stress from reactive oxygen species and various adipokine productions that play a major role in the pathogenesis of NASH. Another theory for NAFLD

progression to NASH is “distinct hit” with pathogenetic heterogeneity obtained via at least 2 different ways: genetic predisposition and timing to activation of different pathways leading simple steatosis to NASH [7].

NAFLD is defined as accumulation of lipid deposits in the hepatocytes in the absence of excessive alcohol consumption and other secondary causes of chronic liver disease, therefore, the diagnosis requires evidence of fatty infiltration in the liver [8]. According to recent guidelines, hepatic fat content determined by histological [9] or biochemical [10] examination of liver biopsy tissue is the gold standard for diagnosing the stages of NAFLD, and for the differentiation of NASH from simple steatosis [11,12]. However, liver biopsy is invasive that carries a small but not negligible risk of complications [13] for assessment of at risk NAFLD patients with major complications occurring in 0.1-2.3% of cases [12].

Thus, it is unsuitable for screening large populations of early stage asymptomatic patients with NAFLD. Furthermore, in both preclinical and clinical pharmaceutical research, repeated liver biopsies are impractical for continuously monitoring disease progression and therapeutic efficacy over the course of treatment. Moreover, since the size of biopsy samples is small, it is subject to sampling error due to sporadic heterogeneous morphological distribution of the pathological changes in the liver, as well as inter-operator variability [13]. Given these limitations, noninvasive imaging methods, such as magnetic resonance [14], computed tomography [15], and ultrasonography [16,17] come into use in the diagnosis and evaluation of NAFLD/NASH.

In contrast to other diagnostic imaging modalities, ultrasonography is safe, noninvasive, non-radioactive, cost effective, convenient to use and widely available. Therefore, ultrasonography appeals to be the most commonly used diagnostic modality in the clinic for detection of NAFLD/NASH with high sensitivity and specificity comparing to other modalities [18]. Especially in large population studies, ultrasound is the primary imaging method widely used for screening asymptomatic patients with increased liver enzymes and suspected NAFLD [19].

In addition to the imaging methods, some serological biomarkers and biometric indices have also been used for noninvasive evaluation of disease progression, e.g., BMI, AST/ALT, and diabetes (BARD) score has been reported to have a high predictive value for advanced fibrosis (stages 3-4) in a population of obese patients in the USA [20]. There are data suggesting that ultrasound and fibrosis-4 (FIB4) indices are probably the most appealing methods for detecting and distinguishing NAFLD/NASH from simple steatosis [21,22]. Cytokeratin 18 fragment (CK-18) levels have been reported as a serological marker of apoptosis associated with NAFLD with positive correlation with histologic steatosis, inflammation, ballooning, fibrosis and total NAFLD activity score [23,24]. Although isolated biomarkers may have limited accuracy for diagnosis and distinguishing NAFLD/NASH from simple steatosis, several algorithms combining multiple biomarkers and risk factors have been developed to improve sensitivity and specificity [25].

In laboratory studies, a major limitation in studying the pathogenesis of NAFLD/NASH has been the lack of translational animal models with metabolic disorders and diabetes. Although some rodent and rabbit models have been used, the outcomes from these models are often not very translatable to the mechanisms of human disease [26]. Naturally occurring T2D in nonhuman primates (NHP) exhibits clinical features of obesity, insulin resistance, dyslipidemia, diabetes, and pancreatic pathology that are similar to those observed in human, thus, has been used as the most translatable animal model for studying the pathophysiologic mechanisms, as well as for testing novel therapies, for metabolic diseases and diabetes [27-36].

The aim of the present study was to test the hypothesis that, similar to humans, spontaneously developed obese, dysmetabolic and diabetic NHPs may also be associated with hepatic histopathologic changes, such as lipidosis, inflammation and fibrosis that would eventually progress to NAFLD/NASH. We 1) adapted a clinical ultrasonography method for noninvasive detection of hepatic histopathologic changes in NHPs; 2) used computer-assisted analysis to quantify the ultrasound images; and 3) examined the correlation of some commonly used ultrasound parameters with accompanying NAFLD/NASH risk factors and biomarkers, such as biometric, blood chemistry and liver fibrosis indices in these NHPs.

Methods

Experiments were carried out in 36 cynomolgus macaques (*Macaca fascicularis*) of either gender without history of pharmaceutical treatment in the past 3 months, and with stable physiological conditions. These animals were individually housed in the animal facility at room temperature ~21°C and a 12 hour light/dark cycle (7:00-19:00), with access to water ad libitum, and fed twice daily with a nutritionally balanced monkey diet (Shanghai Shilin Biotechnology, Inc., Shanghai, China) enriched with seasonal fruits and vegetables. The experimental protocol was in accordance with the guidelines of Association for Assessment and Accreditation of Laboratory Animal Care (AAALAC) and approved by the Institutional Animal Care and Use Committee (IACUC) at Crown Bioscience, Inc.

On the experimental day, each monkey was fasted overnight and anesthetized with an intramuscular injection of ketamine (Fujian Gutian Pharmaceutical Co. Ltd., Fujian, China) at an initial dose of 10 mg/kg followed by 5 mg/kg as needed. Body temperature was maintained at ~37°C by a thermostatically controlled warm water-circulating pad placed underneath the body. Throughout the experimental period, animals were monitored for vital signs which may trigger intervention (supportive and/or emergent care) and/or study termination, including: oxygen saturation <90%; body temperature <35°C; heart rate <100 or >200 beats/min; respiratory rate <20 or >60/min, serious arrhythmia and respiratory artifacts, etc.

Biometric and body fat composition measurements

Biometric measurements: The animal was placed in a sitting and vertical position with the abdomen at natural and straight position without external force and extrusion. The waist circumference (WC) was measured around the umbilicus. Height was measured by the summation of the length of 3 segments: crown to rump, rump to knee, and knee to plantar surface. Body mass index (BMI) was calculated by the formula:

$$\text{BMI} = \text{body weight (kg)} / \text{height (crown to plantar surface, meter)}^2 \quad (1)$$

Body fat composition: The total body (Total-fat) and trunk (Trunk-fat) fat composition was assessed by a Dual Energy X-ray Absorptiometry (DXA, GE densitometer, Lunar I DEXA Promodel). Anesthetized animal had all metal objects removed and was placed on a bed in supine position remaining motionless for scanning. After the full body scan, a software (Lunar encore 2011, version 13.6) was used to calculate the fat, bone and other mass for different regions of the entire body. The android region was measured around the waist area, between the midpoint of the lumbar spine and the top of the pelvis. The gynecoid area was measured approximately between the femoral head and the mid-thigh. The software demarcated and separated the limbs from the torso and from the head by standard lines generated by the equipment itself; these lines were adjusted according to specific anatomical points determined by the manufacturer. The Total-fat or Trunk-fat (%) was calculated as below:

$$\text{Fat composition (\%)} = \frac{\text{fat mass}}{\text{total body mass}} \times 100 \quad (2)$$

Ultrasonography examination and computer assisted imaging analysis

Each monkey was examined using the ultrasound system (Pro Sound SSD-3500SX, Hitachi Aloka Medical, Ltd. Tokyo, Japan) with a 3.5-5 MHz convex transducer by 2 different radiologists blinded to the

metabolic status of the animals during scanning and imaging analysis. All the instrument settings, including “gain”, “depth”, “time-gain compensation”, etc. were fixed for each measurement. After completion of the above measurements, animals were returned to their home cage and closely monitored by trained personnel until completely recovered from anesthesia, when the animals were placed in the upright position and food and water provided. Representative images of the liver, kidney and surrounding organs were captured at different defined angles and stored on a computer hard disk for offline imaging analysis to obtain 186 parameters that represent different pathophysiological status of hepatic lipodosis and other morphological changes based on commonly used clinical methods. All digitized ultrasound images were analyzed by 2 radiologists involved in scanning, using Image J software (version 1.41, NIH, Bethesda, MD).

Hepatic/renal echo-intensity ratio (H/R, Figure 1A and 1B) In a sagittal view of the liver and right kidney of the lateral position, the echogenicity of the right kidney was used as a reference for identification of liver parenchyma. A 1.5 × 1.5 cm uniform region of interest (ROI) in the liver parenchyma was selected, excluding blood vessels, bile ducts, and other focal hypo/hyper echogenicity. Another 0.75 × 0.75 cm ROI was obtained in the cortex of the right kidney with no large vessels, renal sinus or medulla. To avoid interference of depth-dependent echo-intensity attenuation and borderline echo distortion effects, the boundary between the liver and right kidney area was placed near the center of the image, and the ROIs of the liver and right kidney were selected at the same depth of the ultrasound images. The gray scales for the 2 ROIs were measured by the total pixels as respective hepatic and renal echo-intensities for calculation of H/R ratio 37. In order to reduce the sampling noise resulting from heterogenic distribution of histopathological changes, 3 ROIs in the liver and kidney were obtained for an average H/R ratio.

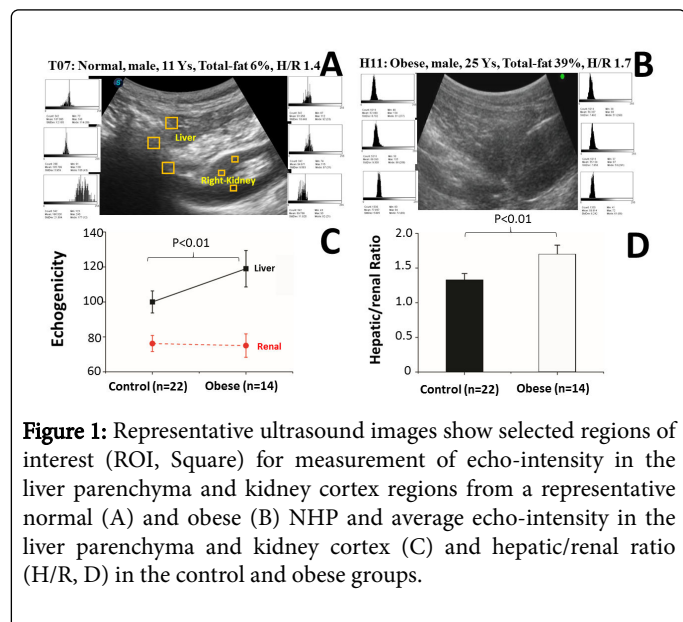


Figure 1: Representative ultrasound images show selected regions of interest (ROI, Square) for measurement of echo-intensity in the liver parenchyma and kidney cortex regions from a representative normal (A) and obese (B) NHP and average echo-intensity in the liver parenchyma and kidney cortex (C) and hepatic/renal ratio (H/R, D) in the control and obese groups.

Hepatic echo-intensity attenuation rate (HA, Figure 2A and 2B) In a right subcostal view at the anterior axilla line under supine position, a tangent line was drawn and the ultrasound wave transmission line was determined, starting from the point of tangency and perpendicular to the tangent line. Two ROIs of 1.5 × 1.5 cm were selected in homogeneous hepatic regions along the ultrasound transmission line near and posterior to the liver anterior margin, with a distance of 4-6

cm in depth. The actual linear distance between the 2ROIs was also measured for HA calculation38.

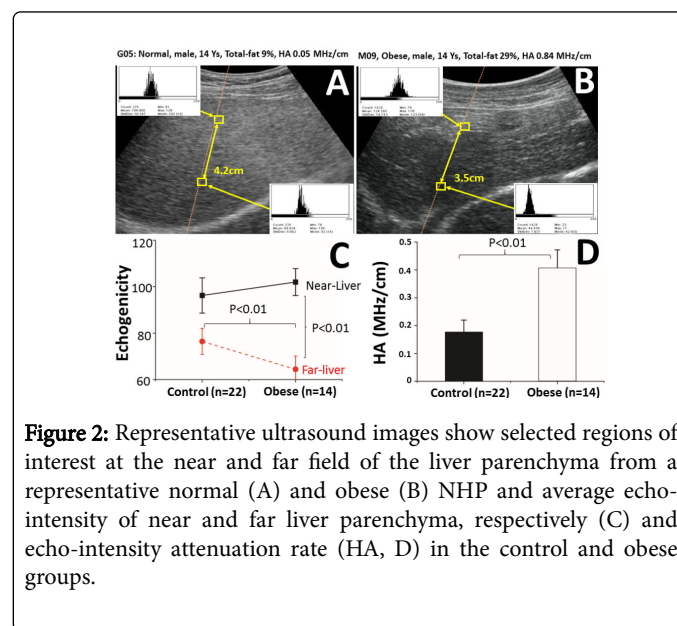


Figure 2: Representative ultrasound images show selected regions of interest at the near and far field of the liver parenchyma from a representative normal (A) and obese (B) NHP and average echo-intensity of near and far liver parenchyma, respectively (C) and echo-intensity attenuation rate (HA, D) in the control and obese groups.

The echo-intensity of ultrasound waves was attenuated exponentially, shown as the following equations where A_0 and A_d are echo-intensities at the sound source and the liver parenchyma at a specific depth, respectively; a is the attenuation coefficient of the liver parenchyma; f is the frequency of the ultrasound detector; and d is the depth of ROI38:

$$A_d = A_0 \times e^{-a \cdot f \cdot d} \quad (3)$$

The ratio of the average echo-intensity for the ROIs in the near- (A_n) to far- (A_f) field of 217 the liver obtained from equation (3) is then calculated as below, where d_n and d_f are the depth of 218 near- and far-field ROIs in the liver, respectively.

$$\frac{A_n}{A_f} = e^{a \cdot f \cdot (d_f - d_n)} \quad (4)$$

Then the formula for hepatic echo-intensity attenuation rate deduced from equation (4) is 221 calculated as below where Δd is the distance between the near- and far-field ROIs.

$$HA = \frac{(\ln A_n - \ln A_f)}{(\Delta d \cdot f)} \quad (5)$$

Liver triglyceride content measurement and histopathology examinations

Liver tissues obtained in the tissue bank from several previous necropsy normal and dysmetabolic/diabetic NHPs were fixed in formalin (10% neutral buffered), embedded in paraffin wax blocks and 5 μm in thickness sections were stained with hematoxylin-eosin-safran About 100 mg liver tissue was homogenized for 30 seconds in 5% NP40 (Beyotime, China) with protease inhibitor cocktail (sigma, USA), centrifuged at 12,000 g/min for 2 minutes for collection of the supernatant. The samples were tested by a triglyceride quantification kit (Bio Vision, USA).

Liver fibrosis panel

Many noninvasive panels of tests have been developed to stage liver disease, including a combination of clinical and routine laboratory parameters, as well as specialized tests involving direct biomarkers of fibrosis and elastography [21-24], among which are

Fibrosis-4 index(FIB4)=Age (y) × AST (IU/L)/(platelet counts (10⁹/L) × vALT (IU/L)) (6)

BARD score (scale 0-4): BMI ≥ 28 kg/m²=1, AST/ALT ≥ 0.8=2, T2D=1 (7)

AST to platelet ratio index (APRI) = AST (IU/L) / platelet count (10⁹/L) × 100 (8)

Cytokeratin 18-fragment (CK-18) was measured by a monkey cytokeratin 18 ELISA kit (My BioSource, US). Whole blood was collected into an ice-cold K2-EDTA tube; plasma separated by centrifugation at 3000 rpm for 15 min at 4°C and stored in -80°C until analysis.

Statistical analysis

All the data were expressed as mean ± standard error (SE). Statistical analysis was conducted using SPSS 17.0 software for Windows (version 17.0; IBM-SPSS, Chicago, Illinois, USA). Student t-tests were used to compare the mean values between the 2 groups. Univariable logistic regression analysis was conducted to examine the relationships between the prevalence of H/R ratio or HA and other risk factors with odds ratios (OR) and 95% confidence intervals (CI) being used to examine the associations between animals with or without certain risk factors. Because there is no consensus for the criteria of these risk factors in NHPs, we determined the threshold using 3 methods: 1) based on our experience in an NHP population arbitrarily set: age ≥ 10 years; Total- & Trunk-fat ≥ 20%; fasting blood glucose (FBG) ≥ 85 mg/dL; glycosylated hemoglobin A1C (HbA1c) ≥ 6%; 2) the median values of the populations in the present study were used due to abnormal distribution of the data: BMI ≥ 13.5 kg/m², BW ≥ 9.3 kg, WC ≥ 45 cm, platelet count ≥ 310 × 10⁹/L, CK-18 ≥ 13 ng/ml, FIB4 ≥ 0.36, APRI ≥ 0.46, H/R ratio ≥ 1.4, HA ≥ 0.19 MHz/cm; 3) based on the literature: ALT ≥ 40 and 31 U/L and AST ≥ 37 and 31 U/L for males and females, respectively; CHO ≥ 200 mg/dL; TG ≥ 150 mg/dL; HDL ≤ 35 mg/dL; LDL ≥ 140 mg/dL; BARD ≥ 2. Relationships between the dependent and independent variables in the individual animals were analyzed using simple linear regression. All P-values were 2-sided and considered statistically significant when less than 0.05.

Results

General characterizations (Table 1)

The study consisted of 36 cynomolgus monkeys of both genders with age ranging from 5-21 years, BW 4.2-17.2 kg, BMI 8.2-24.7 kg/m², WC 28.5-78.0 cm, Total-fat 4.1-53.6%, Trunk-fat 15.8-25.4%, H/R ratio 0.79-2.60, HA -9.9-71.0 kHz/cm, ALT 20-176 IU/L, AST 14-83 IU/L, Platelet counts 237-519 × 10⁹/μL, CHO 72-200 mg/dL, TG 25-297 mg/dL, HDL 19-76 mg/dL, LDL 15-91mg/dL, FBG 34-255mg/dL, HbA1c 3.9-10.2%, CK-18 2.1-4.5 ng/mL, FIB4 0.04-0.39, APRI 0.09-1.38, BARD 0-4. The animals were divided into control and obese groups with Total-fat composition being set at 20%. As expected, general characteristics of the NHPs, including BW, BMI, WC, Total- and Trunk-fat, TG, LDL as well as the liver fibrosis indices:

BARD score, APRI and AST/ALT, were all significantly higher in the obese compared to control group.

	Total-fat<20% (n=22)	Total-fat ≥ 20% (n=14)	p value
General Characterizations			
Age (years)	12.2 ± 1.1	12.6 ± 0.9	0.415
BW(kg)	8.5 ± 0.5	10.8 ± 0.8	0.008
BMI (kg/m ²)	12.5 ± 0.5	15.5 ± 1.0	0.002
WC (cm)	40.9 ± 1.5	53.0 ± 2.6	0.000
Total-fat (%)	9.8 ± 1.2	29.6 ± 2.6	0.000
Trunk-fat (%)	11.3 ± 1.5	35.2 ± 2.5	0.000
FBG (mg/dL)	107.4 ± 10.8	116.7 ± 18.2	0.248
HbA1c (%)	6.5 ± 0.6	5.1 ± 0.4	0.067
CHO (mg/dL)	117.6 ± 6.4	105.3 ± 4.7	0.125
HDL (mg/dL)	46.8 ± 3.3	49.5 ± 2.5	0.273
LDL (mg/dL)	50.5 ± 4.0	37.2 ± 5.0	0.043
TG (mg/dL)	84.5 ± 8.8	135.6 ± 25.0	0.008
Liver Fibrosis Indices			
FIB4	0.3 ± 0.1	0.4 ± 0.1	0.121
BARD	1.7 ± 0.3	3.1 ± 0.3	0.001
APRI	0.40 ± 0.05	0.55 ± 0.11	0.017
CK-18 (ng/mL)	11.8 ± 1.8	14.3 ± 3.5	0.491
ALT (IU/L)	55.1 ± 7.4	41.4 ± 6.1	0.010
AST (IU/L)	42.8 ± 4.0	56.6 ± 9.8	0.040
Platelet (10 ⁹ /μL)	313.9 ± 26.5	300 ± 30.3	0.279

Table 1: Characterization of obese monkeys.

Liver triglyceride contents and histopathological characterizations

In 3 control and 4 diabetic NHPs, postmortem necropsy was carried out to collect the liver tissues for measurement of liver tissue triglyceride content as well as histopathology analysis. The liver TG contents were significantly higher in the diabetic than control group (Figure 3A), which were strongly correlated with fasting blood glucose (Figure 3B). The gross appearance of the livers was yellowish with stiff texture. HE staining showed a clear fatty accumulation in the hepatocytes of the liver from the dysmetabolic NHPs (Figure 4). Some of them had diffuse fatty changes with micro and macro vacuoles, especially in the liver with severe fatty accumulation, hepatocyte ballooning was recognized. Mild inflammatory cell infiltration in the fatty liver was also recognized mostly in the portal area. Mild and focal fibrosis appeared in the portal, central vein and peri-sinusoidal areas, especially in the liver with severe fatty changes. Bridge fibrosis and cirrhosis were not observed at this stage.

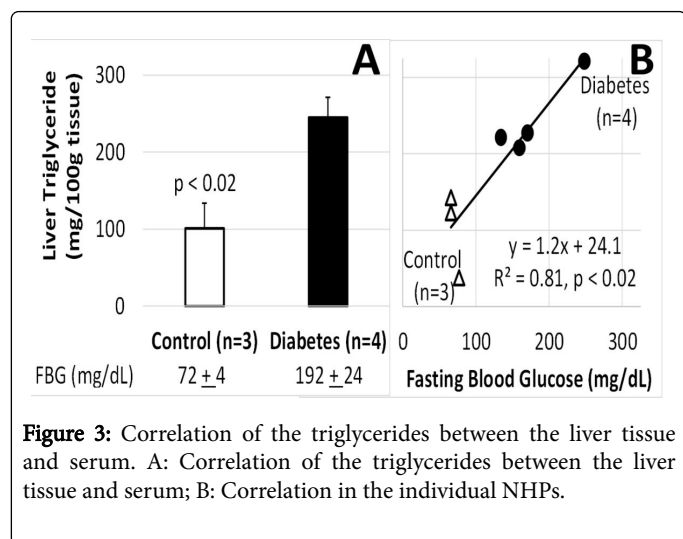


Figure 3: Correlation of the triglycerides between the liver tissue and serum. A: Correlation of the triglycerides between the liver tissue and serum; B: Correlation in the individual NHPs.

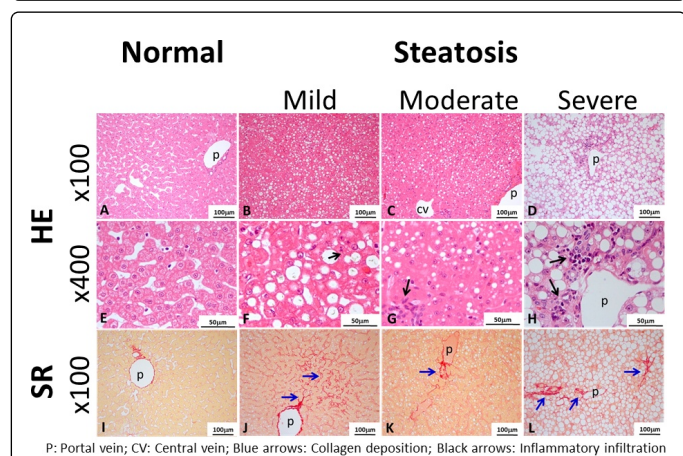


Figure 4: Postmortem histopathology of the liver tissues from a normal and 3 dysmetabolic monkeys at different stages of steatosis/steatohepatitis. Top (low magnification = x 50); and Middle (high magnification = x400): Hematoxylin and eosin H and E) stain shows different stages of steatosis/steatohepatitis with black arrows indicating inflammatory cell infiltrations, p: portal vein; cv: central vein. A & E: Normal liver; B & F: Mild steatotic liver with micro vacuoles and very few inflammatory cell infiltrations; C & G: Moderate steatotic liver with micro vacuoles and many inflammatory cell infiltrations widely and forming a focus; D & H: Severe steatotic liver with macro vacuoles and significant hepatocyte ballooning degeneration, multiple foci of inflammatory cell infiltrations; Bottom: Sirius red (SR) stain (magnification = x100) for collagen depositions indicated by blue arrows; p: portal vein; I: Original collagen deposited only in the portal area; J: Slightly enlarged area of collagen deposition in the portal area, several areas of 566 hepatocyte basement membrane showed an enhanced collagen intensity without pathological collagen deposition; K: Slightly enlarged area of collagen deposition in the portal area, but no intracellular deposition; L: Enlarged area of collagen deposition in the portal area, and several focal intracellular collagen depositions.

Echography characterizations and correlation with metabolic and liver fibrosis indices

The liver parenchyma from a control NHP (Figure 1A and 2A) had homogeneous echo texture with similar or a slightly higher echogenicity when compared to the parenchyma of the kidney cortex and spleen. Fatty liver (Figure 1B and 2B) showed greater echogenicity (bright liver) than the kidney cortex and spleen parenchyma. The echography was analyzed digitally for correlation with biometrical and metabolic status as well as liver fibrosis indexes as below.

	H/R<1.4 (n=20)	H/R ≥ 1.4 (n=16)	p value
General Characterization			
Age (years)	12.1 ± 0.8	12.6 ± 1.3	0.359
BW(kg)	9.5 ± 0.6	9.1 ± 0.8	0.334
BMI (kg/m ²)	13.6 ± 0.6	13.8 ± 0.9	0.100
WC (cm)	44.8 ± 1.9	46.7 ± 3.0	0.292
Total-fat (%)	16.5 ± 2.5	18.8 ± 3.4	0.276
Trunk-fat (%)	19.4 ± 3.0	22.1 ± 3.9	0.281
FBG(mg/dL)	111.1 ± 14.2	119.9 ± 12.6	0.049
HbA1c (%)	5.1 ± 1.0	5.9 ± 0.9	0.117
CHO (mg/dL)	116.4 ± 6.5	108.4 ± 5.5	0.182
HDL(mg/dL)	47.0 ± 3.2	49.8 ± 3.0	0.334
LDL(mg/dL)	46.6 ± 4.3	43.8 ± 5.3	0.342
TG (mg/dL)	100.0 ± 17.2	110.6 ± 17.6	0.051
Liver Fibrosis Indices			
FIB4	0.25 ± 0.0	0.61 ± 0.1	0.000
BARD	1.5 ± 0.3	3.2 ± 0.2	0.000
APRI	0.26 ± 0.03	0.70 ± 0.08	0.000
CK-18 (ng/mL)	13.8 ± 2.7	11.5 ± 2.1	0.529
ALT (IU/L)	38.2 ± 5.2	59.1 ± 7.9	0.022
AST (IU/L)	34.8 ± 3.9	65.0 ± 7.3	0.001
Platelet (10 ⁹ /μL)8	340.8 ± 17.1	270.9 ± 37.4	0.039
Liver Ultrasound			
HA (kHz/cm)	6.6 ± 2.3	31.5 ± 4.4	0.006

Table 2: Characterization of monkeys for hepatic/renal echo-intensity ratio (H/R).

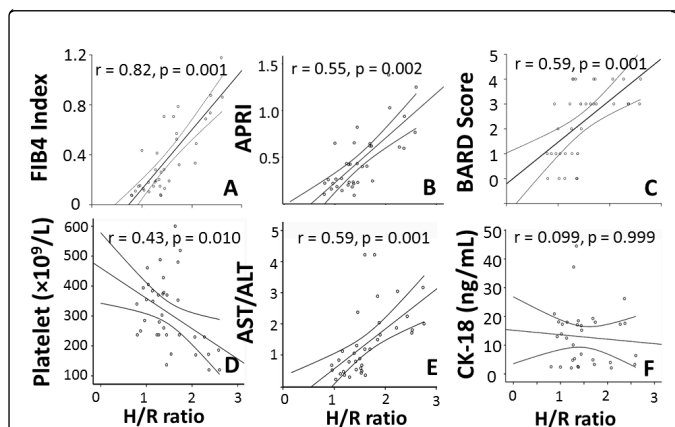


Figure 5: Correlation between hepatic/renal echo-intensity ratio (H/R) with liver fibrosis indices: A. Fibrosis-4 (FIB4); B. AST to Platelet Ratio Index (APRI); C. BMI, AST/ALT ratio, Diabetes score (BARD); D. Platelet counts; E. ASL/ALT ratio; F. Serum cytokeratin 18 fragment (CK-18).

Hepatic/renal echo-intensity ratio (H/R, Figure 1) The average echo-intensity for the liver parenchyma, but not the kidney cortex was significantly higher (Figure 1C), hence the greater H/R ratio (Figure 1D) in the obese than control group. Linear regression analysis revealed a strong positive correlation (Figure 5) between the H/R ratio and the liver fibrosis indices such as FIB4 (A), APRI (B), BARD (C), platelet counts (D), and AST/ALT ratio (E), but not with CK-18 (F). When divided the NHPs by H/R ratio lower or higher than 1.4, there was no significant differences in the general characterizations between the 2 groups; however, the animals with high H/R ratio had significantly higher liver fibrosis indexes except for CK-18, and lower platelet counts than those with low H/R ratio (Table 2).

	HA < 14.6 KHz/cm (n=18)	HA ≥ 14.6 KHz/cm (n=18)	p value
General Characterization			
Age (yr)	11.1 ± 1.0	13.6 ± 0.9	0.037
BW(kg)	9.1 ± 0.7	9.6 ± 0.7	0.299
BMI (kg/m ²)	13.2 ± 0.7	14.1 ± 0.8	0.172
WC (cm)	43.8 ± 2.1	47.4 ± 2.6	0.144
Total-fat (%)	14.1 ± 2.6	20.9 ± 3.0	0.043
Trunk-fat (%)	16.6 ± 3.1	24.6 ± 3.5	0.044
FBG(mg/dL)	104.8 ± 12.5	118.2 ± 14.6	0.257
HbA1c (%)	6.1 ± 0.6	5.7 ± 0.6	0.612
CHO (mg/dL)	117.2 ± 7.4	108.5 ± 4.6	0.163
HDL(mg/dL)	46.3 ± 3.8	49.3 ± 2.4	0.051
LDL(mg/dL)	48.6 ± 4.5	42.1 ± 4.8	0.172
TG (mg/dL)	94.3 ± 16.4	115.5 ± 17.8	0.048
Liver Fibrosis Indices			
FIB4	0.2 ± 0.03	0.5 ± 0.07	0.000
BARD	1.7 ± 0.3	2.8 ± 0.3	0.013
APRI	13.4 ± 2.3	23.3 ± 3.3	0.009
CK-18 (ng/mL)	14.5 ± 3.5	11.7 ± 1.7	0.431
ALT (IU/L)	45.3 ± 6.1	54.2 ± 8.5	0.019
AST (IU/L)	34.9 ± 3.8	61.4 ± 7.2	0.001
Platelet (10 ⁹ /μL)	340.8 ± 17.1	270.9 ± 37.4	0.039
Liver Ultrasound			
H/R ratio	1.2 ± 0.1	1.8 ± 0.1	0.000

Table 4: Characterization of monkeys for hepatic echo-intensity attenuation rate (HA).

	OR	95% CI for OR	p value
General Characterization			
Age (>10 years)	1.4	0.3-5.6	0.636
BW(>9.3 kg)	1.9	0.5-7.1	0.366
BMI (>13.5 kg/m ²)	4.1	1.0-16.6	0.049
WC (> 45cm)	1.6	0.4-5.9	0.503
Total-fat (>20%)	6.5	7.2-5.7	0.017
Trunk-fat (>20%)	3	0.8-11.9	0.065
FBG (>85 mg/dL)	1.7	1.0-2.4	0.047
HbA1c (>6%)	1.7	1.0-2.5	0.037
CHO (>200 mg/dL)	1.2	0.3-4.4	0.821
HDL (<35 mg/dL)	1	0.3-3.6	0.940
LDL (>140 mg/dL)	0.8	0.4-1.0	0.506
TG (>150 mg/dL)	3.8	2.9-4.8	0.030
Liver Fibrosis Indices			
FIB4 (>3.6)	19.8	3.2-120.0	0.001
BART (>2)	27.9	3.0-257.3	0.003
APRI (>0.46)	5	1.2-20.9	0.028
CK-18 (>13 ng/mL)	0.9	0.2-3.6	0.881
ALT (>40(male), 31 (female) IU/L)	1.2	1.0-1.9	0.041
AST (>37(male), 31(female) IU/L)	3.2	1.2-5.2	0.000
Platelet count (>310 x 10 ⁹ /μL)	0.3	0.1-0.2	0.091
Liver Ultrasound			
HA (≥ 14.6 kHz/cm)	2.4	0.6-9.2	0.002

Table 3: Univariable and multivariable analysis of the risk factors associated with hepatic/renal echo-intensity ratio (H/R).

Furthermore, at a defined threshold for each risk factor, the univariable and multivariable analysis revealed that BMI, Total-fat, FBG, HbA1c, TG, HA, as well as the liver fibrosis indices except for CK-18 and platelet counts were significantly associated with H/R ratio (Table 3). Hepatic echo-intensity attenuation rate (HA, Figure 2). The average echo-intensity diminished more when the ultrasound penetrated from the surface to a deep site of the liver, thus, resulting in a significantly greater decay in the echo-intensity (Figure 2C), thus higher HA (Figure 2D) in the obese than control group. When the NHPs were divided into 2 groups with HA above or below 14.6 kHz/cm, the animals with high HA were significantly older and more obese, with higher TG and all the liver fibrosis indices except for CK-18, and lower platelet counts than those with low HA (Table 4). Univariable and multivariable analysis revealed higher prevalence rates of WC, Total-&Trunk-fat, and some liver fibrosis indices such as FIB4 index, BART score and AST/ALT, were significantly associated with HA (Table 5). Furthermore, there was a strong positive correlation between the H/R ratio and HA (Tables 2-5).

	OR	95%CI for OR	p value
General Characterization			
Age (>10 yr)	2.8	0.66-11.92	0.164
BW(> 9.3 kg)	2	0.52-7.69	0.313
BMI (>13.5 kg/m ²)	3.1	0.8-12.3	0.100
WC (>45 cm)	2	1.3-3.7	0.010
Total-fat (>20 %)	7.9	1.7-37.4	0.010
Trunk-fat (>20 %)	5.2	1.3-21.6	0.023
FBG (>85 mg/dL)	1	0.9-4.3	0.049
HbA1c (>6 %)	1	0.2-4.4	1.000
CHO (>200 mg/dL)	1	0.3-3.7	1.000
HDL(>35 mg/dL)	0.4	0.07-2.8	0.379
LDL (>140 mg/dL)	0.9	0.1-1.8	0.877
TG (>150 mg/dL)	0.3	0.06-1.17	0.047
Liver Fibrosis Indices			
FIB4(>3.6)	6.2	1.3-29.4	0.020
BART (>2)	4.4	1.0-18.6	0.046
APRI (>0.46)	3.3	0.8-13.0	0.096
CK-18 (>13 ng/mL)	0.7	0.2-2.7	0.598
ALT (>40 (male), 31 (female) IU/L)	0.7	0.2-2.4	0.503
AST (>37 (male), 31 (female) IU/L)	8	1.4-45.4	0.019
Platelet count (>310 × 10 ⁹ /μL)	1.3	0.3-4.6	0.739
Liver Ultrasound			
H/R ratio ≥ 1.4)	13	2.6-65.2	0.002

Table 5: Univariable and multivariable analysis of the characteristics associated with hepatic echo-intensity attenuation rate (HA).

Discussion

The present study demonstrated for the first time that similar to human patients, spontaneously developed obese, dysmetabolic and T2D cynomolgus monkeys also display characteristics of NAFLD/NASH, including high BW, BMI, WC, and hyperlipidemia (TG & LDL) accompanied by elevated H/R ratio and HA (echography) as well as some liver fibrosis indices such as FIB-4, APRI, BART, AST/ALT, etc. Liver histology represented steatotic hepatitis with focal fibrosis. In parenchymal liver disease, ultrasound reflections from the liver tissue are altered, mainly resulting from intracellular accumulation of fat vacuoles, inflammatory infiltration, fibrosis formation, structure destruction such as hepatomegaly and vascular blurring of the portal or hepatic veins, etc.12. In the clinic, with noninvasive echography, steatosis can be qualitatively assessed by: 1) “bright liver”: hyper-echogenicity of the liver tissue often compared to hypo-echogenicity of the kidney cortex; 2) greater decay of echo intensity with depth (posterior beam attenuation); 3) fine, tightly packed echoes; and 4) loss of echo reflections from the wall of the portal vein, etc. (featureless appearance) [16,17]. In the present study, the clinical echography method has been adapted for application in NHP model of obese, dysmetabolism and diabetes. Although our data also showed a bright liver in obese NHPs (Figure 1A and 1B, Figure 2A and 2B), such detection is traditionally a qualitative or semi-quantitative scoring method, highly dependent on the examiner’s subjective experience for interpretation. This can lead to diagnostic errors and limitations for reproducibility; therefore, objective and quantitative approaches for identification of patients and following-up the degree of disease progression have been suggested [40]. Computer-assisted echography analysis has been developed for quantification of liver echography images in clinical application [41]. Increased H/R ratio has been reported in obese compared to normal-weight children [37]; which is strongly correlated with hepatic fat content measured radioactively [38,39] and the degree of histologic steatosis with liver biopsy [40-42], as well as being significantly distinguishable in NAFLD patients from healthy controls [43]. When ultrasound penetrates into the liver tissue, the echo-intensity decays proportionally with the distance (depth). In a diseased liver with fatty accumulation, inflammatory infiltrations, fibrosis and structure destruction, there would be a greater decay in echogenicity, measured by the hepatic echo- intensity attenuation rate (HA). Indeed, in NAFLD/NASH patients, an elevated HA also strongly correlates with an increase in hepatic fat content measured by 1H-MRS [44]. Consistent with these clinical observations, the present data demonstrated for the first time that both H/R ratio and HA were also significantly greater in obese NHPs, which was highly correlated with many risk factors related to obesity, dysmetabolism, diabetes and liver disease. Furthermore, H/R ratio and HA are also highly correlated with each other, indicating that both indices may reflect similar morphological changes in the liver. Additional echography features, such as hepatorenal contrast (the difference in echogenicity between the liver and right kidney cortex) or blurring of the hepatic vein have similar sensitivity whereas other characteristics such as portal vein blurring or posterior attenuation have lower sensitivity [43]. Also consistent with our observations in the cynomolgus monkeys, we also observed similar liver echo graphic changes in spontaneously developed obese, dysmetabolic and T2D rhesus monkeys (data not shown). Furthermore, Wang et al. reported a similar correlation between the noninvasive ultrasound detection and the clinical progression of both biochemical and pathological changes from liver biopsy samples in rhesus monkeys with alcohol-induced liver steatosis and fibrosis [45]. The liver fibrosis panel has been used clinically as a

biomarker for the noninvasive assessment of liver function and structure changes, including liver enzymes AST/ALT, CK-18, platelet counts, and other metabolic risk factors, such as age, BW, BMI, gender, hypertension, diabetes, etc. Among these risk factors, FIB4, BARD, APRI, etc. were reported to have high sensitivity and specificity for the diagnosis of advanced liver fibrosis in the NAFLD population [22,23,38]. In consistent with these clinical reports, the present data also showed increased ALT/AST, FIB4, BARD, and APRI, as well as reduced platelet counts, indicating a compromised liver function and structure in the NHPs with high H/R ratio and HA. In particular, our data demonstrate d strong correlations between H/R ratio and all 3 liver fibrosis indices, indicating that computer-assisted echography may quantitatively reflect both the liver function as well the degree of histopathological changes in the liver tissue in NHPs with NAFLD/NASH. No significant correlation of CK-18 with the echography, metabolic and liver fibrosis indices suggests that this may not be a sensitive marker in the NHP model, or that liver pathologic changes are still in the early disease stage. This is consistent with the clinical report that CK-18 levels significantly elevated only in NAFLD patients when liver histological changes reached stages 3-5. In summary, the noninvasive sonography with computer-assisted imaging analysis realized the objective quantification of characteristics of NAFLD/NASH, which showed enormous advantages over traditional qualitative methods. The quantitative echography parameters were able to identify the minimal echogenicity changes for “bright liver” that, otherwise, would not be possible to distinguish by the naked eye. They are objective and less dependent on operators’ subjective impression and judgement, thus, could overcome the errors resulting from subjective bias. Therefore, it provides an ideal tool in both largescale clinical investigations in patients and preclinical studies in experimental animal models, such as NHPs to follow-up efficacy of the therapeutic agents during the course of the treatment for NAFLD/NASH. Furthermore, the similar pathogenic characteristics and accompanied risk factors observed in both humans and monkeys make the current NHP model of spontaneously developed obesity, dysmetabolism and diabetes a unique translational tool not only for studying the pathogenic mechanisms of disease progression, but also for testing novel pharmacological interventions for diabetes related NAFLD/NASH.

- All the coauthors are significantly contributed to this work, carefully reviewed and agreed to submit this manuscript for publication.
- YQ Liu and HH Gu contributed equally.
- Part of the data in this manuscript have been presented in 2016 ADA meeting and the abstract has been subsequently published in the proceedings of Diabetes Journal.
- The authors gratefully acknowledge the excellent technical assistance of QM Shao, QX Kong and other vivarium staffs for their professionally caring the NHPs and assisting in the experiments.
- There is no external financial support to this work and no conflict interests with all the authors.

Compliance Statement

There is no external research fund was received by any authors in this article, thus, the authors have no conflict of interest in performing the work for this article. This article does not contain any studies with human participants or using human tissues. The study protocol in using experimental animal model was in accordance with the

guidelines of Association for Assessment and Accreditation of Laboratory Animal Care (AAALAC) and approved by the Institutional Animal Care and Use Committee (IACUC) at Crown Bioscience, Inc.

References

1. Saito K, Uebanso T, Maekawa K, Ishikawa M, Taguchi R, et al. (2015) Characterization of hepatic lipid profiles in a mouse model with nonalcoholic steatohepatitis and subsequent fibrosis. *Scientific reports* 5: 12466.
2. Polyzos SA, Kountouras J, Zavos C, Deretzi G (2012) Nonalcoholic fatty liver disease: multimodal treatment options for a pathogenetically multiple-hit disease. *J Clin Gastroenterol* 46: 272-284.
3. Mohammadi A, Bazazi A, Maleki-Miyandoab T, Ghasemi-Rad M (2012) Evaluation of relationship between grading of fatty liver and severity of atherosclerotic finding. *Int J Clin Exp Med* 5: 251-256.
4. Vernon G, Baranova A, Younossi ZM (2011) Systematic review: the epidemiology and natural history of non-alcoholic fatty liver disease and non-alcoholic steatohepatitis in adults. *Aliment Pharmacol Ther* 34: 274-285.
5. Targher G, Bertolini L, Padovani R, Rodella S, Tessari R, et al. (2007) Prevalence of nonalcoholic fatty liver disease and its association with cardiovascular disease among type 2 diabetic patients. *Diabetes Care* 30: 1212-1218.
6. Leite NC, Salles GF, Araujo AL, Villela-Nogueira CA, Cardoso CR (2009) Prevalence and associated factors of non-alcoholic fatty liver disease in patients with type-2 diabetes mellitus. *Liver Int* 29: 113-119.
7. Yilmaz Y (2012) Review article: is non-alcoholic fatty liver disease a spectrum, or are steatosis and non-alcoholic steatohepatitis distinct conditions? *Aliment Pharmacol Ther* 36: 815-823.
8. Agrawal S, Duseja A (2014) Nonalcoholic Fatty Liver Disease--The Clinician's Perspective. *Trop Gastroenterol* 35: 212-221.
9. Patel NS, Peterson MR, Brenner DA, Heba E, Sirlin C, et al. (2013) Association between novel MRI-estimated pancreatic fat and liver histology-determined steatosis and fibrosis in non-alcoholic fatty liver disease. *Aliment Pharmacol Ther* 37: 630-639.
10. Puri P, Baillie RA, Wiest MM, Mirshahi F, Choudhury J, et al. (2007) A lipidomic analysis of nonalcoholic fatty liver disease. *Hepatology* 46: 1081-1090.
11. Lee SS, Park SH (2014) Radiologic evaluation of nonalcoholic fatty liver disease. *World J Gastroenterol* 20: 7392-7402.
12. Obika M, Noguchi H (2012) Diagnosis and evaluation of nonalcoholic fatty liver disease. *Exp Diabetes Res* 2012: 145754.
13. Cadranet JF, Rufat P, Degos F (2000) Practices of liver biopsy in France: results of a prospective nationwide survey. For the Group of Epidemiology of the French Association for the Study of the Liver (AFEF). *Hepatology* 32: 477-481.
14. Irwan R, Edens MA, Sijens PE (2008) Assessment of the variations in fat content in normal liver using a fast MR imaging method in comparison with results obtained by spectroscopic imaging. *Eur Radiol* 18: 806-813.
15. Duman DG, Celikel C, Tuney D, Imeryüz N, Avsar E, et al. (2006) Computed tomography in nonalcoholic fatty liver disease: a useful tool for hepatosteatosis assessment? *Dig Dis Sci* 51: 346-351.
16. Saverymuttu SH, Joseph AE, Maxwell JD (1986) Ultrasound scanning in the detection of hepatic fibrosis and steatosis. *Br Med J (Clin Res Ed)* 292: 13-15.
17. Joseph AE, Saverymuttu SH, al-Sam S, Cook MG, Maxwell JD (1991) Comparison of liver histology with ultrasonography in assessing diffuse parenchymal liver disease. *Clin Radiol* 43: 26-31.
18. Singh D, Das CJ, Baruah MP (2013) Imaging of non-alcoholic fatty liver disease: A road less travelled. *Indian J Endocrinol Metab* 17: 990-995.
19. Chen CL, Cheng YF, Yu CY, Ou HY, Tsang LL, et al. (2014) Living donor liver transplantation: the Asian perspective. *Transplantation* 97: S3.
20. Harrison SA, Oliver D, Arnold HL, Gogia S, Neuschwander-Tetri BA (2008) Development and validation of a simple NAFLD clinical scoring

- system for identifying patients without advanced disease. *Gut* 57: 1441-1447.
21. Papagianni M, Sofogianni A, Tziomalos K (2015) Non-invasive methods for the diagnosis of nonalcoholic fatty liver disease. *World J Hepatol* 7: 638-648.
 22. Sumida Y, Yoneda M, Hyogo H, Yoshito Itoh, Masafumi Ono, et al. (2012) Validation of the FIB4 index in a Japanese nonalcoholic fatty liver disease population. *BMC Gastroenterol* 12: 2.
 23. Tsutsui M, Tanaka N, Kawakubo M, Sheena Y, Horiuchi A, et al. (2010) Serum fragmented cytokeratin 18 levels reflect the histologic activity score of nonalcoholic fatty liver disease more accurately than serum alanine aminotransferase levels. *J Clin Gastroenterol* 44: 440-447.
 24. Aida Y, Abe H, Tomita Y, Nagano T, Seki N, et al. (2014) Serum cytokeratin 18 fragment level as a noninvasive biomarker for non-alcoholic fatty liver disease. *Int J Clin Exp Med* 7: 4191-4198.
 25. Shen J, Chan HL, Wong GL, Choi PC, Chan AW, et al. (2012) Non-invasive diagnosis of non-alcoholic steatohepatitis by combined serum biomarkers. *J Hepatol* 56: 1363-1370.
 26. Reaven P, Merat S, Casanada F, Sutphin M, Palinski W (1997) Effect of streptozotocin-induced hyperglycemia on lipid profiles, formation of advanced glycation endproducts in lesions, and extent of atherosclerosis in LDL receptor-deficient mice. *Arterioscler Thromb Vasc Biol* 17: 2250-2256.
 27. Hansen BC, Bodkin NL (1986) Heterogeneity of insulin responses: phases leading to type 2 (non-insulin-dependent) diabetes mellitus in the rhesus monkey. *Diabetologia* 29: 713-719.
 28. Bodkin NL, Metzger BL, Hansen BC (1989) Hepatic glucose production and insulin sensitivity preceding diabetes in monkeys. *Am J Physiol* 256: E676-81.
 29. Hansen BC, Bodkin NL (1990) Beta-cell hyperresponsiveness: earliest event in development of diabetes in monkeys. *Am J Physiol* 259: R612-17.
 30. Clark A, de Koning EJ, Hattersley AT, Hansen BC, Yajnik CS, et al. (1995) Pancreatic pathology in non-insulin dependent diabetes (NIDDM). *Diabetes Res Clin Pract* 28: S39-47.
 31. Wagner JE, Kavanagh K, Ward GM, Auerbach BJ, Harwood HJ Jr, et al. (2006) Old world nonhuman primate models of type 2 diabetes mellitus. *ILAR J* 47: 259-271.
 32. Wang XL, Hansen BC, Shi D, Fang Y, Du F, et al. (2013) Quantification of beta-cell insulin secretory function using a graded glucose infusion with C-peptide deconvolution in dysmetabolic, and diabetic cynomolgus monkeys. *Diabetol Metab Syndr* 5: 40.
 33. Xiao YF, Wang BD, Wang XL, Du F, Benzinou M, et al. (2013) Xylazine-induced reduction of tissue sensitivity to insulin leads to acute hyperglycemia in diabetic and normoglycemic monkeys. *BMC Anesthesiol* 13: 33.
 34. Gu HF, Liu YQ, Mei S, Wang B, Sun G, et al. Left ventricular diastolic dysfunction in nonhuman primate model of dysmetabolism and diabetes. *BMC Cardiovasc Disord* 15: 141.
 35. Guo S, Qian WB, Du FL, Wang B, Wang X, et al. (2014) Proteinuria in *Cynomolgus* macaques (*Macaca fascicularis*) with Spontaneously Developed Metabolic Disorder and Diabetes: Transcriptome Analysis of Biopsy Kidney. *J Diabetes Metab* 5: 2-9.
 36. Wang BD, Sun GF, Liu YQ, Qiao J, Ye W, et al. (2016) Dysglycemia and Dyslipidemia Models in Nonhuman Primates: Part II Model of Naturally Occurring and Experimental models of Obesity. *J Diabetes Metab* 7: 641.
 37. Soder RB, Baldisserotto M, Duval da Silva V (2009) Computer-assisted ultrasound analysis of liver echogenicity in obese and normal-weight children. *AJR Am J Roentgenol* 192: W201-205.
 38. Xia MF, Yan HM, He WY, et al. (2012) Standardized ultrasound hepatic/renal ratio and hepatic attenuation rate to quantify liver fat content: an improvement method. *Obesity (Silver Spring)* 20: 444-452.
 39. Expert Panel on Detection E, Treatment of High Blood Cholesterol in Adults (2001) Executive Summary of The Third Report of The National Cholesterol Education Program (NCEP) Expert Panel on Detection, Evaluation, And Treatment of High Blood Cholesterol In Adults (Adult Treatment Panel III). *JAMA* 285: 2486-2497.
 40. Smith-Levitin M, Blickstein I, Albrecht-Shach AA, Goldman RD, Gurewitsch E, et al. (1997) Quantitative assessment of gray-level perception: observers' accuracy is dependent on density differences. *Ultrasound Obstet Gynecol* 10: 346-349.
 41. Saadeh S, Younossi ZM, Remer EM, Gramlich T, Ong JP, et al. (2002) The utility of radiological imaging in nonalcoholic fatty liver disease. *Gastroenterology* 123: 745-750.
 42. Webb M, Yeshua H, Zelber-Sagi S, Santo E, Brazowski E, et al. (2009) Diagnostic value of a computerized hepatorenal index for sonographic quantification of liver steatosis. *AJR Am J Roentgenol* 192: 909-914.
 43. Von Volkman HL, Havre RF, Loberg EM, Haaland T, Immervoll H, et al. (2013) Quantitative measurement of ultrasound attenuation and Hepato-Renal Index in Non-Alcoholic Fatty Liver Disease. *Med Ultrason* 15: 16-22.
 44. Mathiesen UL, Franzen LE, Aselius H, Resjö M, Jacobsson L, et al. (2002) Increased liver echogenicity at ultrasound examination reflects degree of steatosis but not of fibrosis in asymptomatic patients with mild/moderate abnormalities of liver transaminases. *Dig Liver Dis* 34: 516-522.
 45. Wang H, Tan T, Wang J, Niu Y, Yan Y, et al. (2015) Rhesus monkey model of liver disease reflecting clinical disease progression and hepatic gene expression analysis. *Sci Rep* 5: 15019.